Strong influence of El Niño Southern Oscillation on flood risk around the world

Philip J. Ward[a,b,1], Brenden Jongman[a,b], Matti Kummu[c], Michael D. Dettinger[d,e], Frederiek C. Sperna Weiland[f], and Hessel C. Winsemius[f]

[a]Institute for Environmental Studies and [b]Amsterdam Global Change Institute, VU University Amsterdam, 1081 HV Amsterdam, The Netherlands; [c]Water and Development Research Group, Aalto University, 02150 Espoo, Finland; [d]Climate Atmospheric Sciences and Physical Oceanography Division, Scripps Institution of Oceanography, La Jolla, CA 92093; [e]United States Geological Survey, La Jolla, CA 92093; and [f]Deltares, 2629 HD Delft, The Netherlands

Edited by Peter H. Gleick, Pacific Institute for Studies in Development, Environment, and Security, Oakland, CA, and approved September 22, 2014 (received for review May 27, 2014)

El Niño Southern Oscillation (ENSO) is the most dominant interannual signal of climate variability and has a strong influence on climate over large parts of the world. In turn, it strongly influences many natural hazards (such as hurricanes and droughts) and their resulting socioeconomic impacts, including economic damage and loss of life. However, although ENSO is known to influence hydrology in many regions of the world, little is known about its influence on the socioeconomic impacts of floods (i.e., flood risk). To address this, we developed a modeling framework to assess ENSO's influence on flood risk at the global scale, expressed in terms of affected population and gross domestic product and economic damages. We show that ENSO exerts strong and widespread influences on both flood hazard and risk. Reliable anomalies of flood risk exist during El Niño or La Niña years, or both, in basins spanning almost half (44%) of Earth's land surface. Our results show that climate variability, especially from ENSO, should be incorporated into disaster-risk analyses and policies. Because ENSO has some predictive skill with lead times of several seasons, the findings suggest the possibility to develop probabilistic flood-risk projections, which could be used for improved disaster planning. The findings are also relevant in the context of climate change. If the frequency and/or magnitude of ENSO events were to change in the future, this finding could imply changes in flood-risk variations across almost half of the world's terrestrial regions.

flood risk | El Niño Southern Oscillation | climate variability | global scale | flood hazard

El Niño Southern Oscillation (ENSO) is the most dominant interannual signal of climate variability on Earth (1) and influences climate over large parts of the Earth's surface. In turn, ENSO is known to strongly influence many physical processes and societal risks, including droughts, food production, hurricane damage, and tropical tree cover (2–4). For decision makers it is essential to have information on the possible impacts of this climate variability on society. Such information can be particularly useful when the climate variability can be anticipated in advance, thus allowing for early warning and disaster planning (5). For example, projections carried out in September 2013 already suggested a 75% likelihood that El Niño conditions would develop in late 2014 (6). According to the ENSO forecast of the International Research Institute for Climate and Society and the Climate Prediction Center/NCEP/NWS, dated 9 October 2014, observed ENSO conditions did indeed move to those of a borderline El Niño during September and October 2014, with indications of weak El Niño conditions during the northern hemisphere winter 2014–2015 (iri.columbia.edu/our-expertise/climate/forecasts/enso/current/).

However, to date little is known on ENSO's influence on flood risk, whereby risk is defined as a function of hazard, exposure, and vulnerability (7) and is expressed in terms of socioeconomic indicators such as economic damage or affected people. Although global-scale flood-risk assessments have recently become a hot topic in both the scientific and policy communities, assessments to date have focused on current risks (7–11) or future risks under long-term mean climate change (12, 13). Meanwhile, other recent research suggests that ENSO-related variations of precipitation are likely to intensify in the future (14, 15) and that extreme El Niño events may increase in frequency (16). Hence, an understanding of ENSO's influence on flood risk is vital in understanding both the possible impacts of upcoming ENSO events as well as planning for the potential socioeconomic impacts of changes in future ENSO frequency.

In this paper, we show for the first time to our knowledge that ENSO has a very strong influence on flood risk in large parts of the world. These findings build on previous studies, especially in Australia and the United States, which show that ENSO and other forms of climate variability are strongly related to flood hazard in some regions (17–25). To do this, we developed a modeling framework to specifically assess ENSO's influence on global flood risk. The modeling framework involves using a cascade of hydrological, hydraulic, and impact models (10, 11). Using this model cascade, we assessed flood impacts in terms of three indicators: (*i*) exposed population, (*ii*) exposed gross domestic product (GDP), and (*iii*) urban damage (*Materials and Methods*). A novel aspect of the framework is that we are able to calculate flood risk conditioned on the climatology of all years, El Niño years only, and La Niña years only. This allows us, for the first time to our knowledge, to simulate the impacts of ENSO

Significance

El Niño Southern Oscillation (ENSO) affects hydrological processes around the globe. However, little is known about its influence on the socioeconomic impacts of flooding (i.e., flood risk). We present, to our knowledge, the first global assessment of ENSO's influence on flood risk in terms of economic damage and exposed population and gross domestic product. We show that reliable flood risk anomalies exist during ENSO years in basins spanning almost half of Earth's surface. These results are significant for flood-risk management. Because ENSO can be predicted with lead times of several seasons with some skill, the findings pave the way for developing probabilistic flood-risk projections. These could be used for improved disaster planning, such as temporarily increasing food and medicine stocks by relief agencies.

Author contributions: P.J.W., M.K., M.D.D., and H.C.W. designed research; P.J.W., B.J., F.C.S.W., and H.C.W. performed research; P.J.W. and H.C.W. analyzed data; and P.J.W., B.J., M.K., M.D.D., and H.C.W. wrote the paper.

The authors declare no conflict of interest.

This article is a PNAS Direct Submission.

Freely available online through the PNAS open access option.

[1]To whom correspondence should be addressed. Email: philip.ward@ivm.vu.nl.

This article contains supporting information online at www.pnas.org/lookup/suppl/doi:10.1073/pnas.1409822111/-/DCSupplemental.

on flood risk. The hydrological and impact models have previously been validated for the period 1958–2000 (11). Here, we carried out further validation to assess the specific ability of the model cascade to simulate year-to-year fluctuations in peak river flows and flood impacts and anomalies in peak flows and impacts during El Niño and La Niña years (*SI Discussion, Validation of Hydrological and Hydraulic Models*).

Anomalies in Flood Hazard at the Global Scale

We show that significant anomalies in flood volumes (compared with all years) exist across more than a third of the Earth's land surface (excluding Greenland and Antarctica) during both El Niño and La Niña years, namely 34% during El Niño years and 38% during La Niña years (Fig. 1). In Fig. 1, we show significant anomalies in flood volumes with a return period of 100 y. Statistical significance per cell was assessed by bootstrapping the anomalies ($\alpha = 0.05$, 1,000 repetitions). Field significance of the gridded results was assessed using the binomial distribution (26) and found to be highly significant ($P < 0.001$). In some arid regions, the anomaly in flood volumes is relatively small in absolute terms yet statistically significant. Therefore, in Fig. S1 we also show the absolute anomalies in flood volumes. We also examined anomalies in flood volumes for different return periods, ranging from 5 to 1,000 y (Figs. S2 and S3). The patterns of the anomalies remain similar across different return periods. In *SI Discussion, Validation of Hydrological and Hydraulic Models* we describe the validation of the hydrological and hydraulic models in terms of their ability to simulate relative differences in peak annual discharge between different ENSO phases. Relative differences in simulated extreme discharge between the different ENSO phases are generally simulated well. However, in northern high-latitude regions and parts of Central America correlation of annual maximum discharge between years is relatively low.

A few previous studies have examined ENSO's influence on flood-hazard-related variables in specific region (17–21, 24, 25), especially the United States and Australia, and a comparison between our results and those studies is found in SI Text (*SI Discussion, Comparison with Past Results*). Moreover, relationships have been found globally between ENSO and annual peak discharges (27, 28), but to date no such global scale analysis has been carried out for flood hazard.

Anomalies in Flood Risk at the Globally Aggregated Scale

Next, we examined the influence of ENSO on flood risk at the globally aggregated scale. First, we assessed the correlation (Spearman's) between globally aggregated impacts and the Japan Meteorological Agency's Sea Surface Temperature (JMA SST) anomaly index of ENSO per year (*Materials and Methods*). At this aggregated scale we found no statistically significant correlation for any of the impact indicators (i.e., exposed population, exposed GDP, and urban damage) (Table 1). We also assessed flood risk in terms of annual expected impacts. The

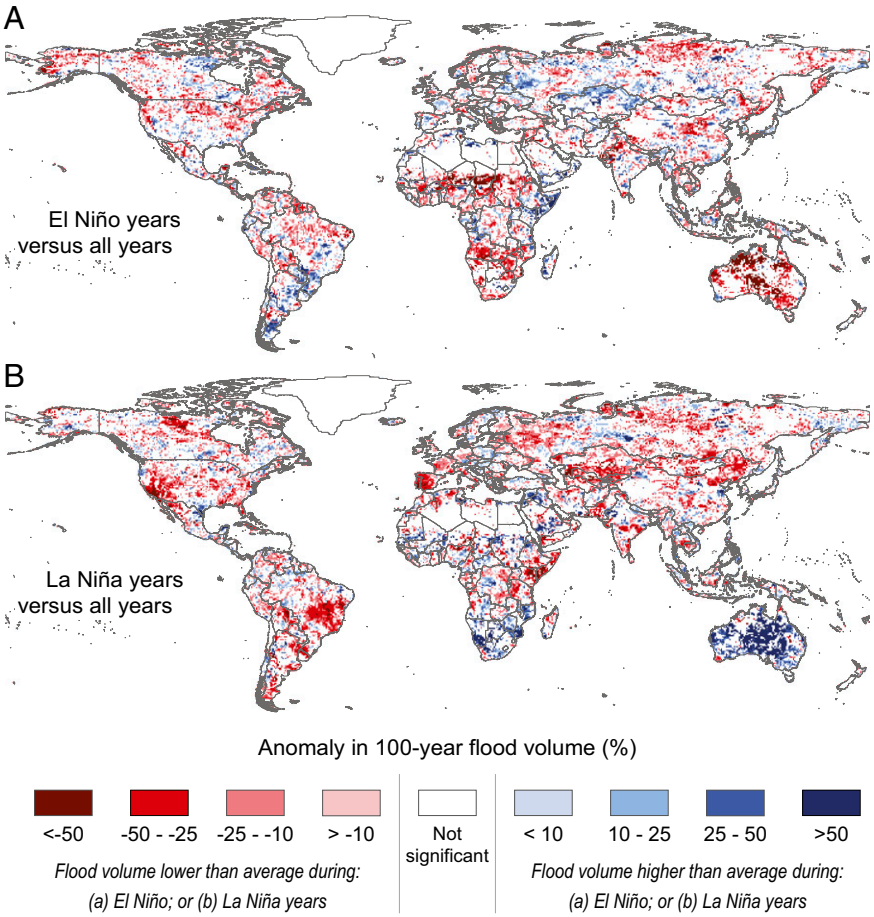

Fig. 1. Percentage anomaly in flood volumes with return periods of 100 y during (*A*) El Niño years and (*B*) La Niña years (compared with all years). Statistical significance per cell was assessed by bootstrapping ($\alpha = 0.05$), using 1,000 repetitions. Field significance of the gridded results was assessed using the binomial distribution (26) and found to be highly significant ($P < 0.001$). Absolute values of the flood anomalies (normalized to area) are shown in Fig. S1. For validation results see *SI Discussion, Validation of Hydrological and Hydraulic Models*.

Table 1. Flood impact results aggregated to the global scale

	Flood risk indicator		
	Exposed population	Exposed GDP	Urban damage
Correlation between impacts per hydrological year and JMA SST_{DJF}			
Rho	−0.14	0.21	0.25
P	0.36	0.18	0.11
Anomalies in annual expected impacts			
El Niño years, %	−8.7	−6.2	−6.8
La Niña years, %	−6.0	−10.2	−14.2

Table shows the correlation (Spearman's rank, rho) between simulated impacts per hydrological year and the JMA SST anomaly index for December–February (JMA SST_{DJF}) and percentage anomalies in simulated annual expected impacts for El Niño and La Niña years (compared with all years).

absolute values based on all years are 154 million people for annual exposed population, $1 trillion [purchasing power parity (PPP)] for annual exposed GDP and $900 billion (PPP) for annual expected urban damage. Compared with these, we found negative anomalies (i.e., lower risk) during both El Niño and La Niña years for all indicators (Table 1). Nevertheless, none of these differences was found to be reliable. Here, reliability refers to whether the annual expected impact at 5th and 95th percentile fits of the Gumbel distribution for El Niño years (or La Niña years) falls outside the range of the corresponding 5th and 95th percentile fits for annual expected impacts from all years (*Materials and Methods*).

These findings are in line with several studies examining relationships between ENSO and flood disasters based on globally aggregated reported loss data. A study of the globally aggregated number of people affected by floods according to the EM-DAT Disaster Events database (29) found no significant correlation with an index of ENSO. Similarly, two studies examining possible relationships between global disaster frequency and ENSO, using data from the US Agency for International Development's Office (30) and EM-DAT (31), found no significant difference between neutral years and El Niño years. It should be noted that the latter study looked at all hydro-meteorological disasters, not just flooding (31), and that the former study only examined El Niño years (not La Niña years) (30).

Anomalies in Flood Risk at the Regional Scale

However, the modeling framework developed here allows us to move beyond globally aggregated results and examine spatially differentiated ENSO influences on flood risk. Regional anomalies in expected annual urban damage in El Niño and La Niña years are shown in Fig. 2, at the scale of food-producing units (FPUs) (32), units that represent a hybrid of countries and river basins. There are differences in the strength and patterns of ENSO influences between the results for urban damage (Fig. 2), exposed GDP (Fig. S4), and exposed population (Fig. S5). These differences are discussed in *SI Discussion*, *Main Differences in Results Between Indicators* and summarized in Table S1. Here, we focus the discussion on the results for urban damage, although it should be noted that for exposed GDP and exposed population there are even more areas with large, reliable anomalies.

Reliable anomalies in expected urban damage exist in at least one ENSO phase (El Niño or La Niña, or both) in FPUs covering 44% of Earth's land area (Fig. 3*A*). At the scale of individual FPUs, the results show particularly strong anomalies in southern Africa, parts of the Sahel and western Africa, Australia, the western United States (especially during La Niña anomalies), and parts of South America (Fig. 2). Strong anomalies were also simulated in parts of Central Eurasia (especially during El Niño), although it should be noted that the validation results show that the model cascade is less reliable in this region (*SI Discussion*, *Validation of Hydrological and Hydraulic Models*).

It is important to note that El Niño and La Niña are associated with both positive and negative anomalies in risk (depending on location and phase). Our simulations revealed reliable anomalies in annual expected urban damage during El Niño years for regions covering 29% of the Earth's land surface, with increased urban damage for 10% and decreased damage for 19%. During La Niña years we simulated reliable anomalies across 23% of the Earth's land surface, with increased damage for 10% and decreased damage for 13%. There are very few areas in which risk is lower during both ENSO phases (<0.1% of land area) or higher during both ENSO phases (<0.1%). We find that asymmetries in annual expected urban damage between ENSO phases are the norm, so that anomalies in annual expected urban damages only switched sign from one ENSO phase (e.g., El Niño) to the other (e.g., La Niña) in FPUs covering 7% of Earth's land surface. If we restrict the analysis only to FPUs with large ENSO-related urban damage anomalies (i.e., anomalies exceeding 25%) we still find ENSO influences in basins covering 40% of the Earth's land surface (Fig. 3*B*). As with the full range of anomalies, we find few areas in which these large anomalies have opposite signs in the two ENSO phases (5%). However, there is a large difference between the total land area with negative anomalies in one ENSO phase and no anomaly in the other phase (26%) vs. those with positive anomalies in one ENSO phase and no anomaly in the other (9%).

Discussion

The results show that for risk assessments it is vital to consider both the positive and negative anomalies in risk associated with ENSO. Reporting of ENSO impacts in the media tends to only focus on its negative effects (see also ref. 31). This may partly explain why a past study on the reported frequency of flood disasters only found significant relationships with ENSO in a handful of countries (30), because that study only examined countries in which disaster frequency was higher during El Niño years and not those where it was lower. Our results thus call for more balanced assessments of ENSO impacts to identify both possible negative and positive affects for society and the economy.

Thus, flood risks associated with ENSO (and, presumably, other global modes of climate variation) show strong, complicated, and societally significant patterns at spatial scales well below that of global aggregations. Indeed, the aggregation scale used to represent anomalies in risk strongly affects the findings. A comparison of anomalies in annual expected flood damage at the country scale (Fig. S6) with those at the FPU scale (Fig. 2) reveals that country-scale assessments mask important regional ENSO influences on risk, especially in large countries where there are subregions that exhibit opposing ENSO influences, such as the United States and Australia. Country-aggregated results indicate no reliable anomaly in the United States during El Niño or La Niña years (Fig. S6), but the regionally (FPU-) disaggregated influences rise to high levels (Fig. 2). Our spatially distributed modeling approach allows us to capture such regional influences in risk, which is not possible using global-scale databases of reported disaster events or losses, because these tend to only list events per country, or at best rudimentary indications of location.

These findings are also relevant to considerations of changing flood risks under a changing climate. Many studies have shown that the frequency and/or intensity of ENSO has varied widely during past millennia to decades (33–36). Our work suggests that such changes in ENSO frequency or intensity, if they recurred in today's world, could have large impacts on flood risk in many regions. Although there is currently no agreement between climate models as to how the frequency of ENSO will change as a result of global warming (37–39), ENSO-related interannual variations of sea-surface temperatures and precipitation are likely to intensify in the future (14, 15), and recent research shows that

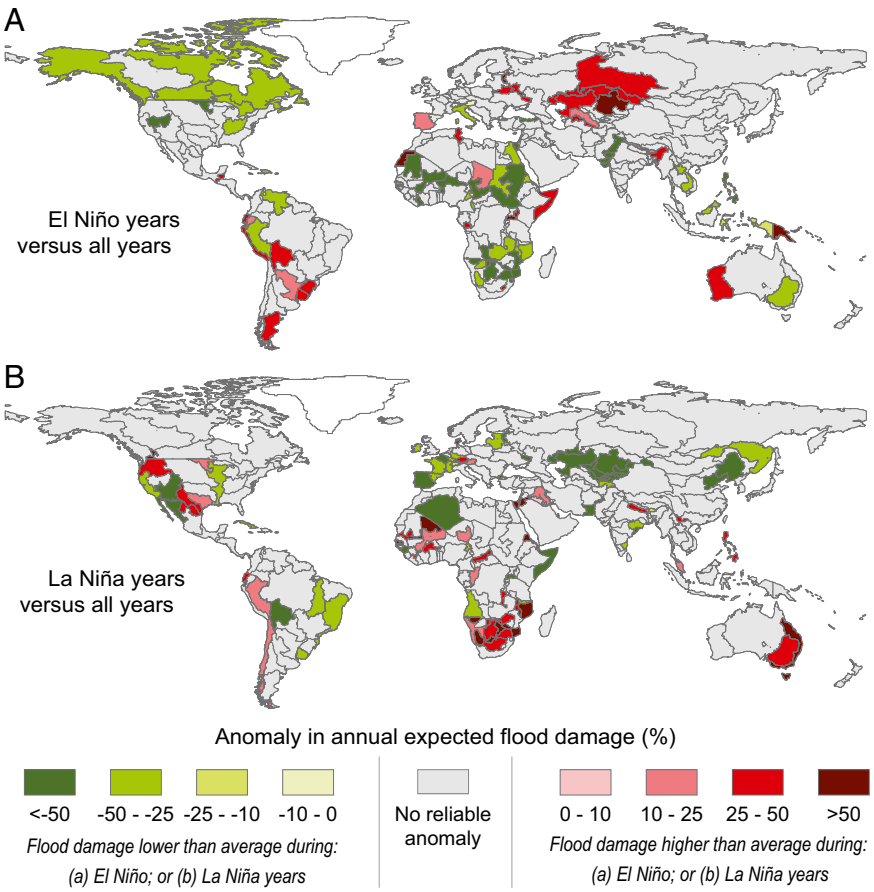

Fig. 2. Percentage anomaly per FPU in annual expected damage in urban areas during (*A*) El Niño years and (*B*) La Niña years (compared with all years). Similar results for annual exposed GDP and annual exposed population are shown in Figs. S4 and S5, respectively. For validation results see *SI Discussion, Validation of Impact Assessment Results*.

extreme El Niño events may increase in frequency (16). If so, given the relationships between ENSO and flood hazard reported here we would anticipate increases in flood risk variability across many, or indeed almost half, of the world's terrestrial regions in the future.

This study is a first attempt to simulate the influence of ENSO on flood risk at the global scale in terms of socioeconomic impacts. We have carried out analyses of the statistical significance in the anomalies in flood volumes and assessed the reliability of the anomalies in risk. The uncertainty of Global Flood Risk with IMAGE Scenarios modeling chain (GLOFRIS) associated with the use of different climate-forcing data and the extrapolation of the extreme value analyses to derive flood volumes up to return periods of 1,000 y has been assessed in ref. 11. Future studies should also attempt to perform full uncertainty analyses. This would require a Monte Carlo-based approach, in which each part of the modeling chain would be rerun with large sets (e.g., 1,000) of different parameter values. This would require the simulation of tens to hundreds of thousands of global flood inundation maps. At the global scale this is not feasible with current computing power. However, in those regions where ENSO impacts on flood risk have been identified more local studies could help to refine our findings and would allow for such full uncertainty assessments.

The implications for risk management are manyfold. For example, the findings have proven useful for the reinsurance industry. In those regions where disaster risk is strongly influenced by ENSO, the spatial and temporal variability in flood risk means that the likelihood of damage claims may increase (or decrease) in particular ENSO phases, affecting the financial resources that need to be reserved to cover losses. It also means that optimal premiums may vary through time, especially in regions where flood damages show strong spatial coherence between nearby basins (40). Moreover, the potential predictability of ENSO (6, 41) might be harnessed to try to account for short-term changes in loss probabilities (42). The findings are also of use to humanitarian institutions. Although humanitarian institutions were established to respond to disasters, there is an increasing discourse on the usefulness of ex-ante actions, especially since the signing of the Hyogo Framework for Action (43). ENSO-based forecasts of increased flood impacts with seasonal lead times could allow for preparatory risk reduction actions to be taken. For example, based on seasonal forecasting of above-normal rainfall in 2008 the International Federation of Red Cross and Red Crescent Societies' regional office in West Africa was able to presource disaster management supplies ahead of time, thereby improving supply availability from about 40 d to 2 d when floods occurred (44). However, this type of action is uncommon, because decision makers are often unable to translate the probability of seasonal above-normal rainfall into a meaningful evaluation in the change of flood or disaster risk (45). The findings from this study explicitly examine changes to such risk and can therefore be more directly translated into appropriate risk reduction actions in El Niño or La Niña years.

When designing actual measures, ideally risk analyses would be carried out for all localities using high-quality datasets, models, and expert knowledge on the ground. However, in practice the models and data required to carry out such analyses only exist in a few regions. In recent years, the value of global-scale risk models to fill this gap and to provide actionable information for flood risk reduction has been demonstrated (7, 46). Because they can provide

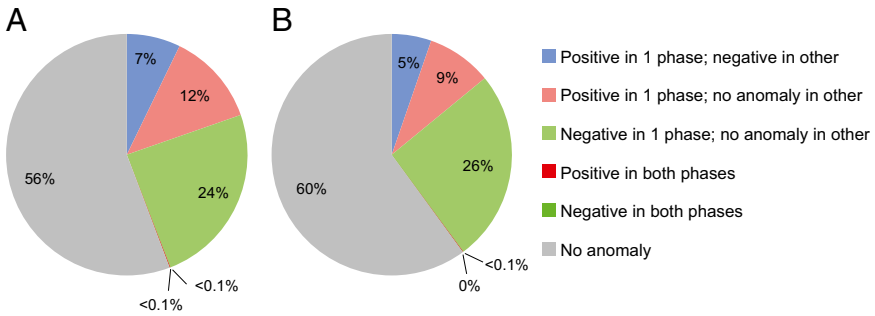

Fig. 3. Percentage of global land area (excluding Antarctica and Greenland) for which there are (*A*) reliable anomalies in annual expected urban damage during either/both El Niño and La Niña years and (*B*) reliable anomalies exceeding 25% in annual expected urban damage during either/both El Niño and La Niña years. For example, "positive in 1 phase; negative in other" means there is a reliable anomaly in either the El Niño or La Niña phase and a negative anomaly in the opposite phase.

information relatively rapidly and cheaply and use consistent methodologies and datasets across different geographical regions, global scale risk assessments can be used to assess the feasibility and prioritization of large-scale strategies before proceeding to local-scale studies.

Materials and Methods

The methods build upon the global flood risk assessment approach described in ref. 11. This approach uses a cascade of hydrological and hydraulic models (10, 11) to simulate inundation extent and depth (in decimeters) at a horizontal resolution of 30 × 30 arcseconds. Two kinds of inundation maps were simulated: (*i*) an inundation map for each hydrological year 1959–2000 and (*ii*) an inundation map for different return periods (5, 10, 25, 50, 100, 250, 500, and 1,000 y) conditioned on all years, El Niño years only, and La Niña years only. The inundation maps were combined with gridded data on urban density, population density, and GDP to estimate flood impacts (11).

More specifically, the method involves (*i*) hydrological and hydraulic modeling to develop daily time series of flood volumes, (*ii*) extreme value statistics to estimate flood volumes for different return periods, (*iii*) inundation modeling for different return periods, and (*iv*) impact modeling. Each step is described below.

Hydrological and Hydraulic Modeling. We simulated daily gridded discharge and flood volume at a horizontal resolution of 0.5° × 0.5° using PCR-GLOBWB-DynRout (47) forced by daily meteorological fields (precipitation, temperature, global radiation) for 1958–2000 from EU-WATCH (48). This procedure is described in ref. 11. This forcing dataset was used because it is the longest temporally consistent global reanalysis dataset currently available at this resolution. Validation of the peak annual discharge results is discussed in *SI Discussion, Validation of Hydrological and Hydraulic Models* and shown in Figs. S7 and S8.

Extreme Value Statistics. From the daily gridded flood volume time series we extracted an annual time series of maximum flood volumes for hydrological years 1959–2000. Here, hydrological years either refer to the period October–September (for most basins) or July–June (for basins in which the flood season occurs in the boreal autumn, i.e., September–November), following the method described in ref. 28. The hydrological years are referred to by the year in which they end, as per standard convention (i.e., hydrological year 1970 refers to the period October 1969 to September 1970). From this, we extracted time series for El Niño and La Niña years only, based on the ENSO classification of the Center for Ocean-Atmospheric Prediction Studies (coaps.fsu.edu/jma.shtml; Table 2). In the original dataset, ENSO years refer to the period October–September, whereby ENSO year 1970 refers to the period October 1970 to September 1971. These were therefore adjusted by 1 y to be consistent with the hydrological year naming convention. We then fit a Gumbel distribution through these three time series (all years, El Niño years, and La Niña years), based on nonzero data, extracting Gumbel parameters for the best-fit and 5th and 95th percentile confidence limits. These Gumbel parameters were then used to calculate flood volumes per grid cell for each return period and for each ENSO phase. Flood volumes were calculated conditioned on the exceedance probability of zero flood volume. For those cells where fewer than five nonzero data points were available in the entire series, flood volume was assumed to be zero.

Inundation Modeling. The coarse-resolution flood volume maps were converted into high-resolution (30- × 30-arcseconds) inundation maps using the GLOFRIS downscaling model (10, 11). First, inundation maps were simulated for each hydrological year (1959–2000) using the annual maps of flood volume from PCR-GLOBWB-DynRout as input. Second, inundation maps were simulated for each return period, conditioned on all years and on El Niño and La Niña years only using the flood volumes derived from the fitted extreme value statistics.

Impact Modeling. Each inundation map was combined with gridded socioeconomic data using the flood impact assessment module (11), which results in a high-resolution (30- × 30-arcseconds) map for each flood impact indicator, namely, exposed population, exposed GDP, and urban damage.

The data and methods used for each specific indicator are described in ref. 11, and in *SI Materials and Methods*. The gridded data can be aggregated to any geographical unit, given the corresponding shapefile. Here, we aggregated the results to the scale of countries and (adapted) FPUs (32), a hybrid of countries and river basins. The simulations produced maps showing impacts for each hydrological year (1959–2000) and also for the different return periods. Annual expected impacts were calculated as the area under an exceedance probability–impact (risk) curve where we assumed that the impact from a 2-y event is zero. Note that the method used assumes that no flood protection measures (e.g., dikes and retention areas that offer protection beyond the 2-y bankfull constraints) are in place. Although the assumption of the flood protection standard has a large influence on the absolute risk estimates (11), we found relative differences between ENSO phases to be fairly insensitive (Table S2). The impact results are validated against reported impacts in *SI Discussion, Validation of Impact Assessment Results* and summarized in Tables S3 and S4.

Statistical Analyses. We assessed correlation between annual hydrological year impacts and JMA SST anomaly index (JMA SST_{DJF}) using Spearman's rank. Significance was assessed by bootstrapping, using 1,000 repetitions. For anomalies in flood volumes between ENSO phases, statistical significance was assessed by bootstrapping the anomalies using 1,000 repetitions. For the annual expected impacts we simulated inundation maps for each return period based on all years, El Niño years, and La Niña years. For each of these we produced inundation maps based on the best fit and the 5th and 95th percentile confidence limits of the Gumbel distribution. We then used these as input to the impact module to estimate impacts for each return period

Table 2. Hydrological years categorized as El Niño and La Niña

ENSO mode	Hydrological year
El Niño	1964, 1966, 1970, 1973, 1977, 1983, 1987, 1988, 1992, 1998
La Niña	1965, 1968, 1971, 1972, 1974, 1975, 1976, 1989, 1999, 2000

Source: coaps.fsu.edu/jma.shtml. Other years are ENSO-neutral. Hydrological and ENSO year classifications are described in *Materials and Methods, Extreme Value Statistics*.

per ENSO phase and for each of the Gumbel fits. We then calculated annual expected impacts for each ENSO phase based on the three Gumbel fits. The anomaly in El Niño (or La Niña) years was calculated as a percentage relative to all years, based on the best-fit. We assessed the reliability of the anomaly based on whether annual expected impacts at 5th and 95th percentile fits for El Niño years (or La Niña years) fell outside the range in corresponding 5th and 95th percentile fits for annual expected impacts from all years. Anomalies in flood volumes per cell between ENSO phases were assessed by bootstrapping the anomalies ($\alpha = 0.05$, 1,000 repetitions). Field significance of the gridded results was assessed using the binomial distribution (26).

ACKNOWLEDGMENTS. We thank the editor and three anonymous reviewers for their valuable comments. We also thank Erin Coughlan (Red Cross/Red Crescent Climate Centre), Alanna Simpson (World Bank Global Facility for Disaster Reduction and Recovery), and Mark Guishard [Risk Prediction Initiative (RPI2.0)] for comments on, and input to, the manuscript. This research was funded by a Veni grant from the Netherlands Organisation for Scientific Research and by a research grant from the RPI2.0 of the Bermuda Institute of Ocean Sciences. Model validation was carried out in the framework of the ENHANCE project (Enhancing risk management partnerships for catastrophic natural hazards in Europe), funded by European Commission Grant 308438. M.K. received funding from Academy of Finland-funded project SCART Grant 267463 (Global green-blue water trajectories and measures for adaptation: linking the Holocene to the Anthropocene). M.D.D. received operational support from the California–Nevada Climate Applications Program, a US National Oceanic and Atmospheric Administration-funded Regional Integrated Science and Assessment program.

1. McPhaden MJ, Zebiak SE, Glantz MH (2006) ENSO as an integrating concept in earth science. *Science* 314(5806):1740–1745.
2. Cane MA, Eshel G, Buckland RW (1994) Forecasting Zimbabwean maize yield using eastern equatorial Pacific sea surface temperature. *Nature* 370:204–205.
3. Pielke RA, Jr, Landsea CN (1999) La Niña, El Niño, and Atlantic hurricane damages in the United States. *Bull Am Meteorol Soc* 80(10):2027–2033.
4. Holgren M, Hirota M, Van Nes EH, Scheffer M (2013) Effects of interannual climate variability on tropical tree cover. *Nat Climate Change* 3:755–758.
5. Coughlan de Perez E, Monasso F, Van Aalst M, Suarez P (2014) Science to prevent disasters. *Nat Geosci* 7:78–79.
6. Ludescher J, et al. (2014) Very early warning of next El Niño. *Proc Natl Acad Sci USA* 111(6):2064–2066.
7. UNISDR (2011) *Global Assessment Report on Disaster Risk Reduction. Revealing Risk, Redefining Development* (United Nations International Strategy for Disaster Reduction Secretariat, Geneva).
8. Jongman B, Ward PJ, Aerts JCJH (2012) Global exposure to river and coastal flooding: Long term trends and changes. *Glob Environ Change* 22(4):823–835.
9. Pappenberger F, Dutra E, Wetterhall F, Cloke H (2012) Deriving global flood hazard maps of fluvial floods through a physical model cascade. *Hydrol Earth Syst Sci* 16: 4143–4156.
10. Winsemius HC, Van Beek LPH, Jongman B, Ward PJ, Bouwman A (2013) A framework for global river flood risk assessments. *Hydrol Earth Syst Sci* 17:1871–1892.
11. Ward PJ, et al. (2013) Assessing flood risk at the global scale: Model setup, results, and sensitivity. *Environ Res Lett* 8(4):044019.
12. Hirabayashi Y, et al. (2013) Global flood risk under climate change. *Nat Clim Change* 3:816–821.
13. Arnell NW, Lloyd-Hughes B (2014) The global-scale impacts of climate change on water resources and flooding under new climate and socio-economic scenarios. *Clim Change* 122(1-2):127–140.
14. IPCC (2013) *Summary for Policymakers. Climate Change 2013: The Physical Science Basis. Contribution of Working Group I to the Fifth Assessment Report of the Intergovernmental Panel on Climate Change* (Cambridge Univ Press, Cambridge, UK).
15. Power S, Delage F, Chung C, Kociuba G, Keay K (2013) Robust twenty-first-century projections of El Niño and related precipitation variability. *Nature* 502(7472):541–545.
16. Cai W, et al. (2014) Increasing frequency of extreme El Niño events due to greenhouse warming. *Nat Clim Change* 4:111–116.
17. Cayan DR, Webb RH (1992) El Niño / Southern Oscillation and streamflow in the western United States. *El Niño: Historical and paleoclimatic aspects of the Southern Oscillation*, eds Diaz HF, Markgraf V (Cambridge Univ Press, Cambridge, UK), pp 29–68.
18. Cayan DR, Redmond KT, Riddle LG (1999) ENSO and hydrologic extremes in the western United States. *J Clim* 12:2881–2893.
19. Waylen PR, Caviedes CN (1986) El Niño and annual floods on the north Peruvian littoral. *J Hydrol (Amst)* 89:141–156.
20. Franks S (2002) Identification of a change in climate state using regional flood data. *Hydrol Earth Syst Sci* 6:11–16.
21. Kiem AS, Franks SW, Kuczera G (2003) Multi-decadal variability of flood risk. *Geophys Res Lett* 30(2):1035.
22. Micevski T, Franks SW, Kuczera GA (2006) Multidecadal variability in coastal eastern Australian flood data. *J Hydrol (Amst)* 327(1-2):219–225.
23. Pui A, Lal A, Sharma A (2011) How does the Interdecadal Pacific Oscillation affect design floods in Australia? *Water Resources Res* 47:W05554.
24. Kiem AS, Verdon-Kidd DC (2013) The importance of understanding drivers of hydroclimatic variability for robust flood risk planning in the coastal zone. *Australian J Water Resources* 17(2):126–134.
25. Ishak EH, Rahman A, Westra S, Sharma A, Kuczera G (2013) Evaluating the non-stationarity of Australian annual maximum floods. *J Hydrol (Amst)* 494:134–145.
26. Livezey RE, Chen WY (1983) Statistical field significance and its determination by Monte Carlo techniques. *Mon Weather Rev* 111(1):46–59.
27. Ward PJ, Beets W, Bouwer LM, Aerts JCJH, Renssen H (2010) Sensitivity of river discharge to ENSO. *Geophys Res Lett* 37(12):L12402.
28. Ward PJ, Eisner S, Flörke M, Dettinger MD, Kummu M (2014) Annual flood sensitivities to El Niño Southern Oscillation at the global scale. *Hydrol Earth Syst Sci* 18:47–66.
29. Bouma MJ, Kovats RS, Goubet SA, Cox JS, Haines A (1997) Global assessment of El Niño's disaster burden. *Lancet* 350(9089):1435–1438.
30. Dilley M, Heyman BN (1995) ENSO and disaster: Droughts, floods and El Niño/Southern Oscillation warm events. *Disasters* 19(3):181–193.
31. Goddard L, Dilley M (2005) El Niño: Catastrophe or opportunity. *J Clim* 18(5):651–665.
32. Kummu M, Ward PJ, De Moel H, Varis O (2010) Is physical water scarcity a new phenomenon? Global assessment of water shortage over the last two millennia. *Environ Res Lett* 5(3):034006.
33. Tudhope AW, et al. (2001) Variability in the El Niño-Southern Oscillation through a glacial-interglacial cycle. *Science* 291(5508):1511–1517.
34. Cobb KM, et al. (2013) Highly variable El Niño-Southern Oscillation throughout the Holocene. *Science* 339(6115):67–70.
35. Li J, et al. (2013) El Niño modulations over the past seven centuries. *Nat Clim Change* 3:822–826.
36. Verdon-Kidd DC, Franks SW (2006) Long-term behaviour of ENSO: Interactions with the PDO over the past 400 years inferred from paleoclimate records. *Geophys Res Lett* 33(6):L06712.
37. Van Oldenborgh GJ, Philip SY, Collins M (2005) El Niño in a changing climate: A multi-model study. *Ocean Sci* 1:81–95.
38. Paeth H, Scholten A, Friederichs P, Hense A (2008) Uncertainties in climate change prediction: El Niño Southern Oscillation and monsoons. *Global Planet Change* 60(3-4): 265–288.
39. Guilyardi E, et al. (2009) Understanding El Niño in ocean–atmosphere general circulation models. Progress and challenges. *Bull Am Meteorol Soc* 90:325–340.
40. Jongman B, et al. (2014) Increasing stress on disaster-risk finance due to large floods. *Nat Clim Change* 4:264–268.
41. Cheng Y, Tang Y, Chen D (2011) Relationship between predictability and forecast skill of ENSO on various time scales. *J Geophys Res* 116:C12006.
42. Merz B, et al. (2014) Floods and climate: Emerging perspectives for flood risk assessment and management. *Nat Hazard Earth Sys* 2:1559–1612.
43. Coughlan de Perez E, et al. (2014) Forecast-based financing: An approach for catalyzing humanitarian action based on extreme weather and climate forecasts. *Nat Hazard Earth Sys Disc* 2:3193–3218.
44. Braman LM, et al. (2013) Climate forecasts in disaster management: Red Cross flood operations in West Africa, 2008. *Disasters* 37(1):144–164.
45. Pagano TC, Hartmann HC, Sorooshian S (2002) Factors affecting seasonal forecast use in Arizona water management: a case study of the 1997-98 El Niño. *Clim Res* 21: 259–269.
46. GFDRR (2014) *Understanding Risk: The Evolution of Disaster Risk Assessment* (World Bank Global Facility for Disaster Reduction and Recovery, Washington, DC).
47. Van Beek LPH, Wada Y, Bierkens MFP (2011) Global monthly water stress: I. Water balance and water availability. *Water Resources Res* 47(7):W07517.
48. Weedon GP, et al. (2011) Creation of the WATCH forcing data and its use to assess global and regional reference crop evaporation over land during the twentieth century. *J Hydrometeorol* 12(5):823–848.

Supporting Information

Ward et al. 10.1073/pnas.1409822111

SI Materials and Methods

The impacts of flooding were calculated using the global flood impact module of GLOFRIS, described in ref. 1. For clarity, we also briefly describe the data and methods used in this impacts module in the following paragraphs. Note that in this paper we used updated versions of the exposure datasets.

Affected Population and Affected GDP. In GLOFRIS, affected population and GDP are estimated using maps showing downscaled population and GDP. For this study, we used maps derived from the IMAGE model (Integrated Model to Assess the Global Environment) (2, 3), which were further downscaled to a horizontal resolution of 30 × 30 arcseconds using LandScan population maps (4). The affected population and GDP were calculated as the sum of the population or GDP located in areas that are shown as flooded in the inundation maps.

Urban Damage. This risk indicator provides an estimate of urban damage, and the calculation uses a map of asset values in urban areas to represent economic exposure and a stage-damage function to represent vulnerability. The asset value map is based on a land-use map, together with an estimate of urban asset values per square kilometer. The land-use data are taken from the HYDE database (5). For each grid cell, HYDE shows the fractional area of land with urban land cover; the horizontal resolution is 5 × 5 arcminutes. Using these data, we calculated the urban area per grid cell at a horizontal resolution of 30 × 30 arcseconds. The next step was to assign an economic value to the urban area per square kilometer data, which was carried out using the method described in ref. 6. Vulnerability was represented by applying a stage-damage function. The function used here is the average of the high and low urban density land-class functions used in the Damagescanner model (7, 8) and can be found in ref. 1. In this paper we specifically estimated relative anomalies in risk during the different phases of ENSO, and hence the choice of the function is not so important. For future analyses looking at absolute risk estimates it is important to account for spatial variations in vulnerability (9).

SI Discussion

Validation of Hydrological and Hydraulic Models. The discharge results of PCR-GLOBWB have been validated in previous studies against observed data on mean monthly discharge (10) and peak annual discharge (1), and the flood volume results of DynRout have been validated against GRACE satellite data of terrestrial water storage (11). In general, the models have been found to show fair to good performance.

In terms of simulating peak annual discharge, the model was previously validated against observed daily discharge data from the Global Runoff Data Centre (GRDC; www.bafg.de/cln_007/nn_266918/GRDC), using gauging stations with daily data availability for more than 25 y (during 1958–2000) and an upstream area above 125,000 km^2. For these stations, the relative error was calculated for discharge with a return period of 10 y, based on extrapolations using the Gumbel distribution fit to the observed and modeled time series. Generally, the relative error was found to be reasonable (between −25 and +25% for 37 of the 53 stations).

However, these validations did not assess the performance of the model in terms of its ability to simulate relative differences in peak discharges between the different phases of ENSO, which is the aspect of most crucial importance for the current paper. Therefore, in this study we carried out extra validation to specifically examine this aspect. We used daily discharge data from the GRDC database, using only those stations with upstream areas greater than 10,000 km^2 for which daily data are available for every day of the hydrological year in at least 15 hydrological years between 1959 and 2000 (i.e., 722 stations).

In Fig. S7 we show the correlation (Spearman's rank) between the modeled and observed values of the maximum daily discharge (Q_{max}) per hydrological year. Generally, the agreement is good. For half of the stations, the correlation coefficient is greater than 0.6, and it is greater than 0.4 for 80% of stations. The correlation is relatively low in northern high-latitude regions. This may be due to earlier noticed biases in the precipitation data in northern latitudes owing to snow undercatch of the used rain gauges (1). Low correlation is also found in several of the gauging stations assessed in Central America.

We also examined the agreement between the modeled and observed data in terms of the relative change in Q_{max} between El Niño and non-El Niño years (Fig. S8*A*) and between La Niña and non-La Niña years (Fig. S8*B*). The figure shows that for the vast majority of stations modeled and observed median Q_{max} show either no significant difference between El Niño (La Niña) and non-El Niño (non-La Niña) years or significant differences of the same sign. For the other stations there is a statistically significant difference in modeled median Q_{max} between El Niño (La Niña) and non-El Niño (non-La Niña) years but none for observed data (or vice versa). There are no stations at which modeled and observed median Q_{max} show significant changes between El Niño/non-El Niño years or La Niña/non-La Niña years with different signs. Hence, the model seems to simulate well the relative differences in peak annual discharge between the different phases.

Validation of Impact Assessment Results. The globally aggregated impact results of the modeling cascade have been validated in ref. 1. For the current paper, we carried out further validation at regionally disaggregated levels, first by the large regions defined in ref. 12 and shown in Table S3 and, second, by country (Table S4). We assessed the correlation (Spearman's rank) between annual reported losses and annual modeled urban damages and between annual reported fatalities and annual modeled exposed population over the period 1990–2000. The reported fatalities and losses were taken from Munich Re's NatCatSERVICE database (13). For this analysis, we only included events for which the main cause of the event is river flooding (i.e., "floods"), and not other forms of floods, for example flash floods, dam breaks, and tsunamis. Both reported and modeled annual impacts were extracted for hydrological years, rather than calendar years. The validation comparisons are intended to give a broad picture of whether the modeled impacts pick up interannual differences in impacts similar to those recorded in the loss database. The modeled and reported impacts are not the same variables (e.g., affected population is compared with reported fatalities). Moreover, loss databases themselves are inherently limited and suffer from many problems; for a detailed discussion see ref. 14. We used the period 1990–2000 only because this is the latest 10-y period for which we have simulated impacts, and the loss database is generally considered to be more reliable for the most recent period compared with early time periods (14).

In Table S3 we show the correlation between annual reported losses and annual modeled urban damages and between annual reported fatalities and annual modeled exposed population for

the world regions. Generally, we see reasonable to good agreement. A major exception is for North Africa, where both pairs of variables show negative correlation. This is not a surprising result for two reasons. First, simulating flood events in this arid region is particularly difficult (1), and second, there are very few reported events in this region ($n = 32$). Hence, we cannot make any statistically robust statements on whether the discrepancy results from the quality of the modeled data or from the reported data, or both. In Eastern Asia, the correlation is almost zero between reported losses and urban damage (rho = 0.52 for reported fatalities and modeled exposed population), and for Eastern Europe and Central Asia the correlation is slightly negative between reported fatalities and modeled exposed population (and positive, although weak, between reported losses and urban damage). For Eastern Europe and Asia, this may be related to the hydrological modeling results: The validation results for modeled vs. observed peak annual discharge (Fig. S7) show low to negative correlation for many gauging stations. The same cannot be said for Eastern Asia, where the discharge validation results are good. The fact that the correlation between reported fatalities and modeled exposed population is reasonably strong in this region, yet the correlation is negative for reported losses vs. urban damage, may be indicative of lower quality of reported loss information. Until recently, many states in the region felt they should not share information of this kind with the rest of the world (14). However, the poor performance for exposed population vs. reported fatalities may simply be due to there being no clear (linear) relationship between these two variables in this region. In our calculations of urban damage we do include a vulnerability component, by means of using a depth-damage function. However, we did not use such a component for exposed population.

The same analysis was carried out using reported and modeled impacts for the 10 countries for which the largest number of reported events are available (Table S4). For most countries, the correlation is again reasonable to strong. An exception is the Russian Federation, and to a lesser extent India. As above, the poor correlation for the Russian Federation may be a result of the fact that our hydrological model does not seem to simulate interannual variations in peak annual discharge very well in this region (compared with observed data), especially in the eastern part. In addition, the Russian Federation and India (as well as many other countries) may have suffered from relatively large numbers of events that remain undocumented, owing to low media penetration and insufficient data collection and sharing. Finally, the reported loss data include both damages in urban and rural areas, whereas the damage model only reflects urban damages. The latter fact may lead to discrepancies in developing countries, such as India, where large parts of the country consist of rural areas and small settlements that are not represented in the global urban density databases.

Comparison with Past Results. ENSO's influence on observed floods has only been examined in a few regions, mainly in the western United States and Australia. An analysis of observed daily discharge data for the Santa Cruz River at Tucson, Arizona (15) showed the magnitude of a 100-y flood to be significantly larger during El Niño years. For the cell in which this river is found, we simulated a positive anomaly in 100-y flood volume (+25%), and for the FPU in which this river is found (Colorado) we simulated a positive anomaly in annual expected damages (+18%). A study of ENSO relationships with peak observed discharges at 303 locations in the western United States (16) found that in El Niño years days with high daily discharge occur more frequently than average over the southwestern United States and less frequently than average over the northwestern United States, with an almost opposite pattern for La Niña years.

We also see this general pattern reflected in our flood-risk results. We found higher exposed population and GDP during El Niño years in the southwestern United States and lower values in the northwest. For urban damage, however, the El Niño signal is weak. During La Niña years, we found lower urban damages, exposed GDP, and exposed population in the southwest and higher urban damages in the northwest. However, the pattern is not clear in basins located in the central part of the western United States. For example, for the Sacramento–San Joaquin basin we simulated negative damage anomalies during La Niña conditions and weak (not reliable) anomalies during El Niño conditions. This is related to hydroclimatological differences between the northern (Sacramento) and southern (San Joaquin) parts of this basin. During La Niña conditions, the simulated anomalies in flood volumes are lower across almost the entire Sacramento–San Joaquin basin, whereas during El Niño conditions negative anomalies are more dominant in most parts of the Sacramento basin, with positive anomalies in most parts of the San Joaquin basin.

For Australia, studies have been carried out to condition flood return periods on indices of ENSO and the Interdecadal Pacific Oscillation (IPO) (17, 18). These studies show graphs of log-normal values of a regional flood index value for New South Wales for return periods between 1 and 100 y, conditioned on El Niño and La Niña years only. The results clearly show higher values of the flood index during La Niña years compared with El Niño years (the climatological mean is not shown). This is in agreement with our maps of flood volume anomalies during La Niña years (positive anomaly) and El Niño years (negative anomalies) in New South Wales. Ishak et al. (19) analyzed a database of annual maximum stream flows in Australia and found that indices of ENSO, IPO, and the Southern Annular Mode can account for most of the observed trend in annual maximum stream flows.

In the northern coastal region of Peru, analyses of observed time series of annual floods for 13 rivers show strong positive peak flow anomalies during El Niño years (20). For this region, we also simulated high positive anomalies in flood volume and damages (+43% for the latter).

Main Differences in Results Between Indicators. We simulated anomalies in risk between the different phases of ENSO for the different risk indicators, namely, annual expected urban damage, exposed GDP, and exposed population. We found that the sign of anomalies is very similar across the different indicators. However, there are clear differences in the strength of the anomalies, and hence also in the number and distribution of reliable anomalies.

In Table S1 we show the percentage of the Earth's land area for which basins showed a reliable positive or negative anomaly during El Niño and/or La Niña years. Note that Antarctica and Greenland are excluded from the analyses. The anomalies per basin are shown in Fig. 2 (annual expected urban damage), Fig. S4 (annual exposed GDP), and Fig. S5 (annual exposed population).

From Table S1 we see large differences in the percentage of land area affected by the different anomalies. For example, during La Niña years similar percentages of land surface experienced positive and negative anomalies (10% and 13% of total land area, respectively). However, for exposed GDP and exposed population, negative anomalies were simulated across much larger areas than is the case for positive anomalies. Figs. S4 and S5 reveal a simple explanation for these differences. For example, during La Niña years, negative anomalies in exposed GDP and population are simulated in the large FPU representing northeastern Russia. However, this anomaly is not simulated for urban damage. For a large part, this explains the difference noted earlier in this paragraph.

A comparison of the maps of anomalies in annual expected urban damage (Fig. 2) with those for annual affected GDP shows, in general, a similar pattern in terms of the signal of the

anomalies. However, there are also some clear differences in terms of the differences in magnitude of the anomalies. Notable differences exist in South America, particularly around the region of the Paraná and San Francisco basins, and in the western basins. In North America, there are several basins in the western and south-central parts of the United States showing reliable anomalies in annual expected urban damage during different ENSO phases, but no anomalies in annual exposed GDP. The strength of the anomalies in southern Africa also tends to be stronger for urban damage than for affected GDP. However, there are regions that show reliable anomalies in affected GDP but no anomalies in urban damage. Further research is required to understand the reasons for these differences, which could be related to several factors. One factor is the location of the exposed elements at risk. So-called urban damages can only occur in regions where urban area is located in flood-prone areas (i.e., where it is potentially exposed to a flood hazard). The same is the case for affected GDP and population. Because the geographical locations of these elements differ, so do the absolute impacts of flooding, and by extension the relative differences between ENSO phases. Another factor of large importance is that the urban damage indicator is dependent on inundation depth, whereas the other indicators are only dependent on the binary presence or absence of inundation. In our approach, the spatial distribution of GDP is directly related to the population density per cell. Hence, the results in ENSO anomalies for these two indicators are very similar.

1. Ward PJ, et al. (2013) Assessing flood risk at the global scale: Model setup, results, and sensitivity. *Environ Res Lett* 8:044019.
2. Van Vuuren DP, Lucas PL, Hilderink H (2007) Downscaling drivers of global environmental change: Enabling use of global SRES scenarios at the national and grid levels. *Glob Environ Change* 17(1):114130.
3. Bouwman AF, Kram T, Klein Goldewijk K (2006) *Integrated Modelling of Global Environmental Change: An Overview of IMAGE 2.4* (Netherlands Environmental Assessment Agency, Bilthoven, The Netherlands).
4. Bright EA, Coleman PR, Rose AN, Urban ML (2010) *LandScan 2010 High Resolution Global Population Data Set* (Oak Ridge National Laboratory, Oak Ridge, TN).
5. Klein Goldewijk K, Beusen A, Van Drecht G, De Vos M (2011) The HYDE 3.1 spatially explicit database of human-induced global land-use change over the past 12,000 years. *Glob Ecol Biogeogr* 20(1):73–86.
6. Jongman B, Ward PJ, Aerts JCJH (2012) Global exposure to river and coastal flooding: Long term trends and changes. *Glob Environ Change* 22(4):823–835.
7. Klijn F, Baan PJ, De Bruijn KM, Kwadijk JC, Van Buren R (2007) Overstromingsrisico's in Nederland in een veranderend klimaat: Verwachtingen, schattingen en berekeningen voor het project Nederland Later (WL | Delft Hydraulics, Delft, The Netherlands).
8. Ward PJ, De Moel H, Aerts JCJH (2011) How are flood risk estimates affected by the choice of return-periods? *Nat Hazard Earth Sys* 11:3181–3195.
9. Jongman B, et al. (2012) Comparative flood damage model assessment: Towards a European approach. *Nat Hazard Earth Sys* 12:3733–3752.
10. Van Beek LPH, Wada Y, Bierkens MFP (2011) Global monthly water stress: I. Water balance and water availability. *Water Resources Res* 47(7):W07517.
11. Wada Y, Van Beek LPH, Bierkens MFP (2012) Nonsustainable groundwater sustaining irrigation: A global assessment. *Water Resources Res* 48(6):W00L06.
12. Kummu M, Ward PJ, De Moel H, Varis O (2010) Is physical water scarcity a new phenomenon? Global assessment of water shortage over the last two millennia. *Environ Res Lett* 5(3):034006.
13. Munich Re (2013) NatCatSERVICE Database (Münchener Rückversicherungs-Gesellschaft, Munich).
14. Kron W, Steuer M, Löw P, Wirtz A (2012) How to deal properly with a natural catastrophe database – analysis of flood losses. *Nat Hazard Earth Sys* 12:535–550.
15. Cayan DR, Webb RH (1992) El Niño / Southern Oscillation and streamflow in the western United States. *El Niño: Historical and Paleoclimatic Aspects of the Southern Oscillation*, eds Diaz HF, Markgraf V (Cambridge Univ Press, Cambridge, UK), pp 29–68.
16. Cayan DR, Redmond KT, Riddle LG (1999) ENSO and hydrologic extremes in the western United States. *J Clim* 12:2881–2893.
17. Kiem AS, Franks SW, Kuczera G (2003) Multi-decadal variability of flood risk. *Geophys Res Lett* 30(2):1035.
18. Kiem AS, Verdon-Kidd DC (2013) The importance of understanding drivers of hydroclimatic variability for robust flood risk planning in the coastal zone. *Australian J Water Resources* 17(2):126–134.
19. Ishak EH, Rahman A, Westra S, Sharma A, Kuczera G (2013) Evaluating the non-stationarity of Australian annual maximum floods. *J Hydrol (Amst)* 494:134–145.
20. Waylen PR, Caviedes CN (1986) El Niño and annual floods on the north Peruvian littoral. *J Hydrol (Amst)* 89:141–156.
21. Livezey RE, Chen WY (1983) Statistical field significance and its determination by Monte Carlo techniques. *Mon Weather Rev* 111(1):46–59.

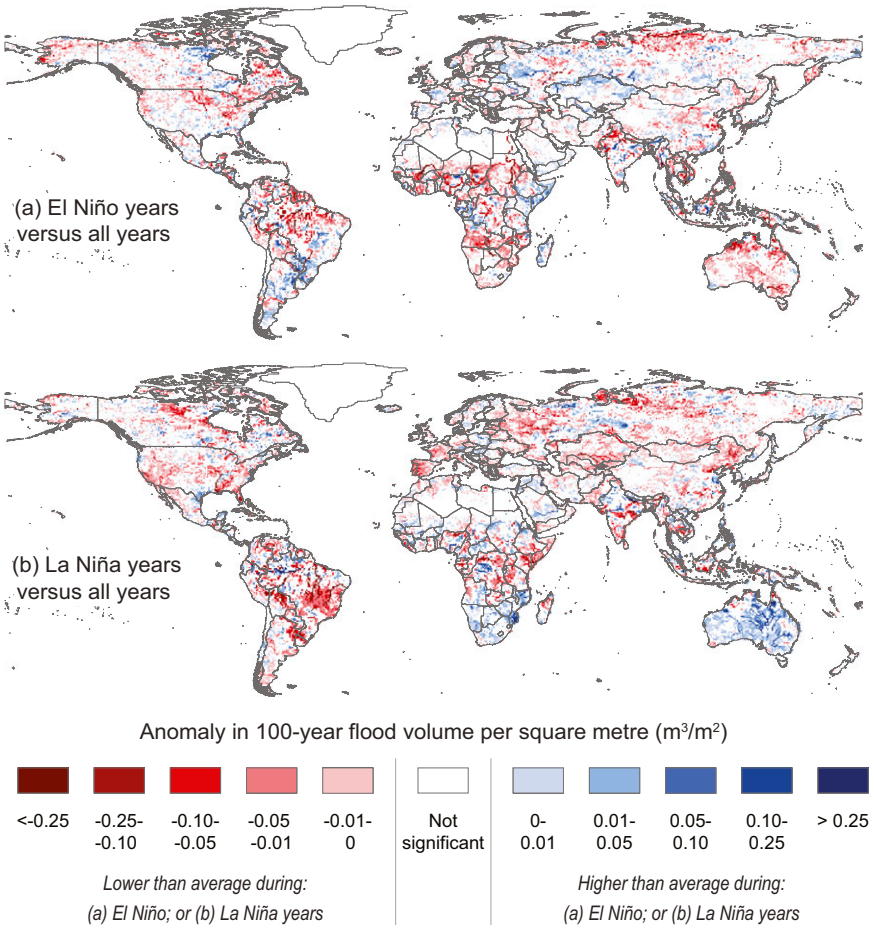

Fig. S1. Absolute anomaly in flood volumes normalized to surface area per cell (cubic meter per square meter) with return periods of 100 y during (*A*) El Niño years and (*B*) La Niña years (compared with all years). Statistical significance was assessed by bootstrapping ($\alpha = 0.05$), using 1,000 repetitions. Field significance of the gridded results was assessed using the binomial distribution (21) and found to be highly significant ($P < 0.001$).

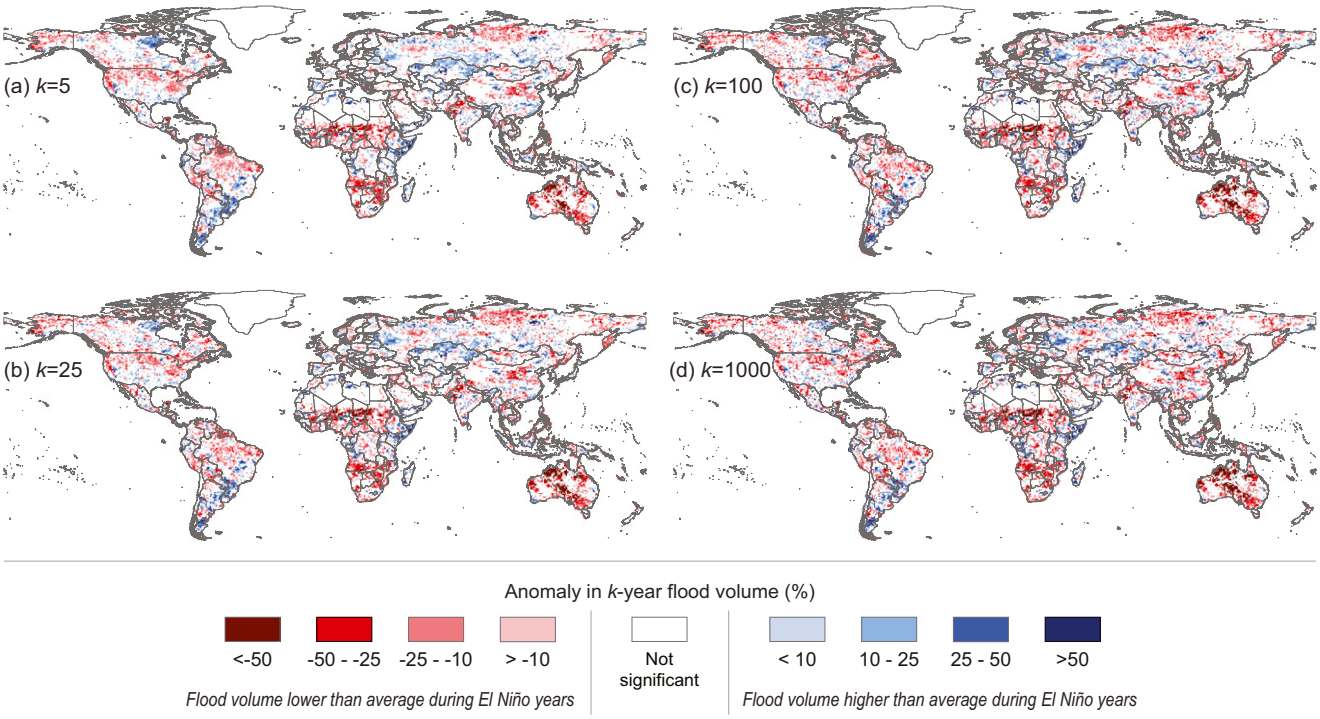

Fig. S2. Percentage anomaly in flood volumes during El Niño years (compared with all years) with a return period of (*A*) 5 y, (*B*) 25 y, (*C*) 100 y, and (*D*) 1,000 y. Statistical significance per cell was assessed by bootstrapping ($\alpha = 0.05$), using 1,000 repetitions. Field significance of the gridded results was assessed using the binomial distribution (21) and found to be highly significant ($P < 0.001$). Compared with the percentage anomalies in flood volumes during El Niño years with a return period of 100 y (Fig. 1*A*), the strengths of the anomalies generally show a small increase for floods with shorter return periods. In most regions this change is very small, and hence there is little change between the categories shown in the figure. The patterns of the anomalies therefore remain similar across different return periods.

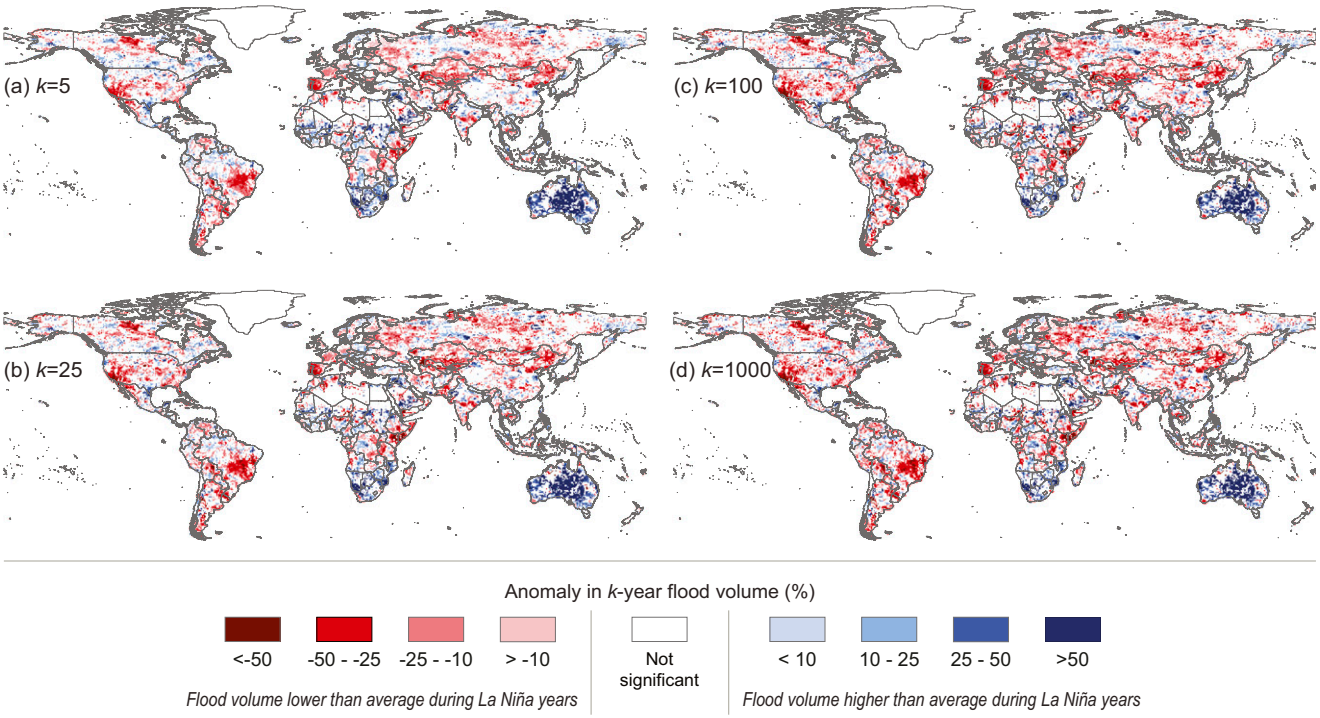

Fig. S3. Percentage anomaly in flood volumes during La Niña years (compared with all years) with a return period of (*A*) 5 y, (*B*) 25 y, (*C*) 100 y, and (*D*) 1,000 y. Statistical significance per cell was assessed by bootstrapping ($\alpha = 0.05$), using 1,000 repetitions. Field significance of the gridded results was assessed using the binomial distribution (21) and found to be highly significant ($P < 0.001$). Compared with the percentage anomalies in flood volumes during La Niña years with a return period of 100 y (Fig. 1*B*), the strengths of the anomalies generally show a small increase for floods with shorter return periods. In most regions this change is very small, and hence there is little change between the categories shown in the figure. The patterns of the anomalies therefore remain similar across different return periods.

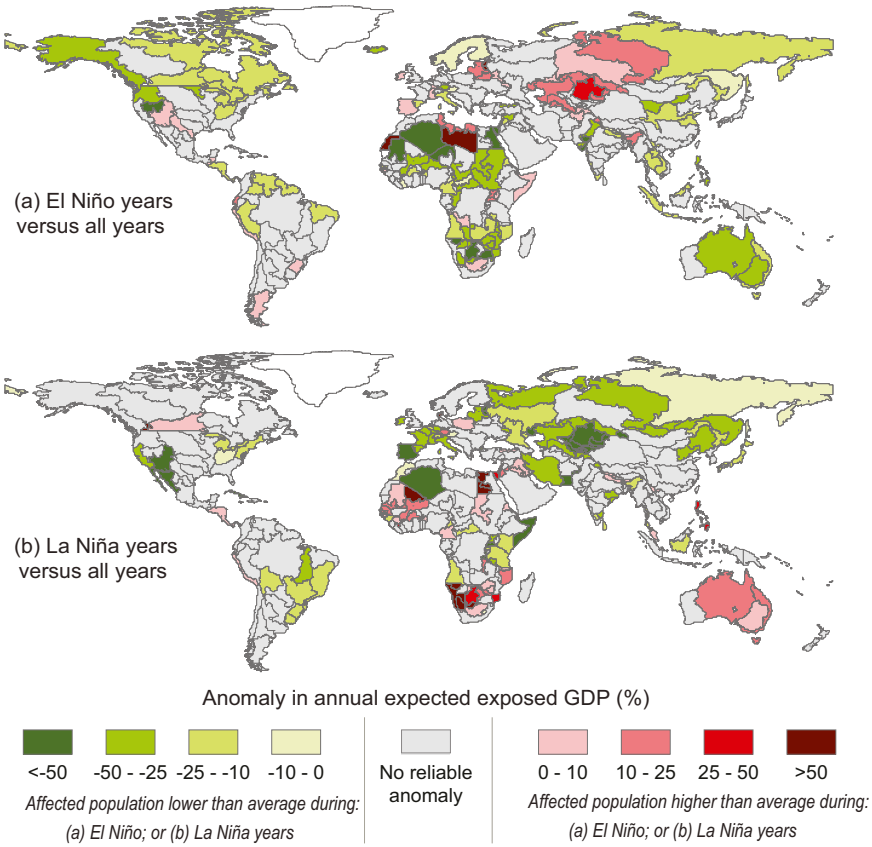

Fig. S4. Percentage anomaly per FPU in annual expected exposed GDP for (*A*) El Niño years and (*B*) La Niña years (compared with all years).

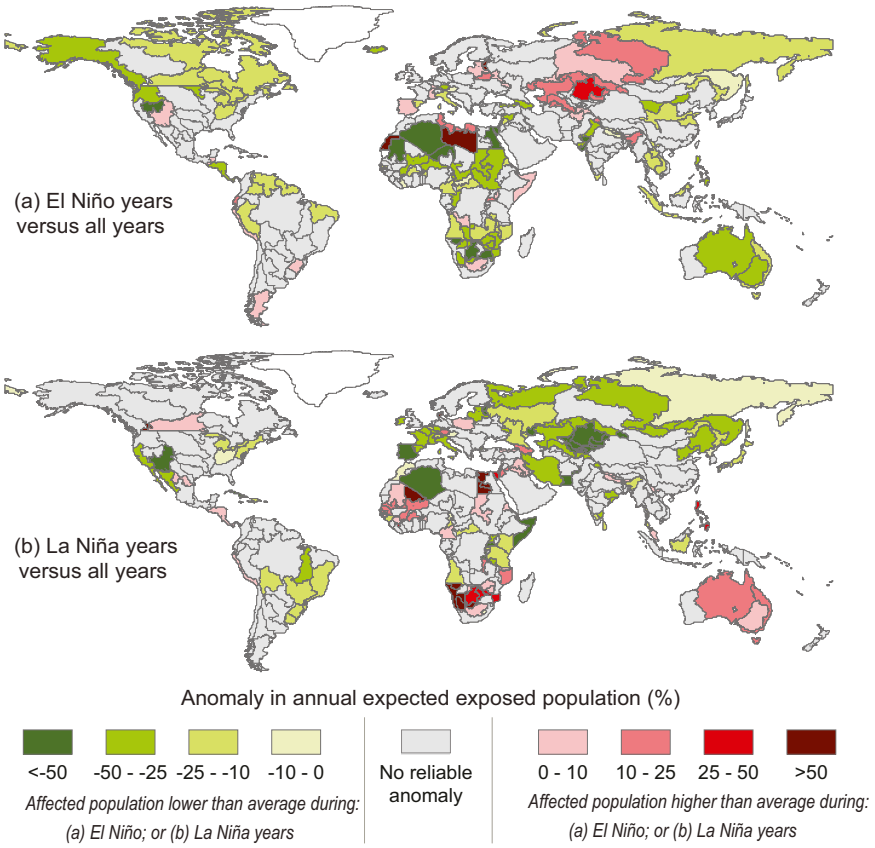

Fig. S5. Percentage anomaly per FPU in annual expected exposed population for (*A*) El Niño years and (*B*) La Niña years (compared with all years).

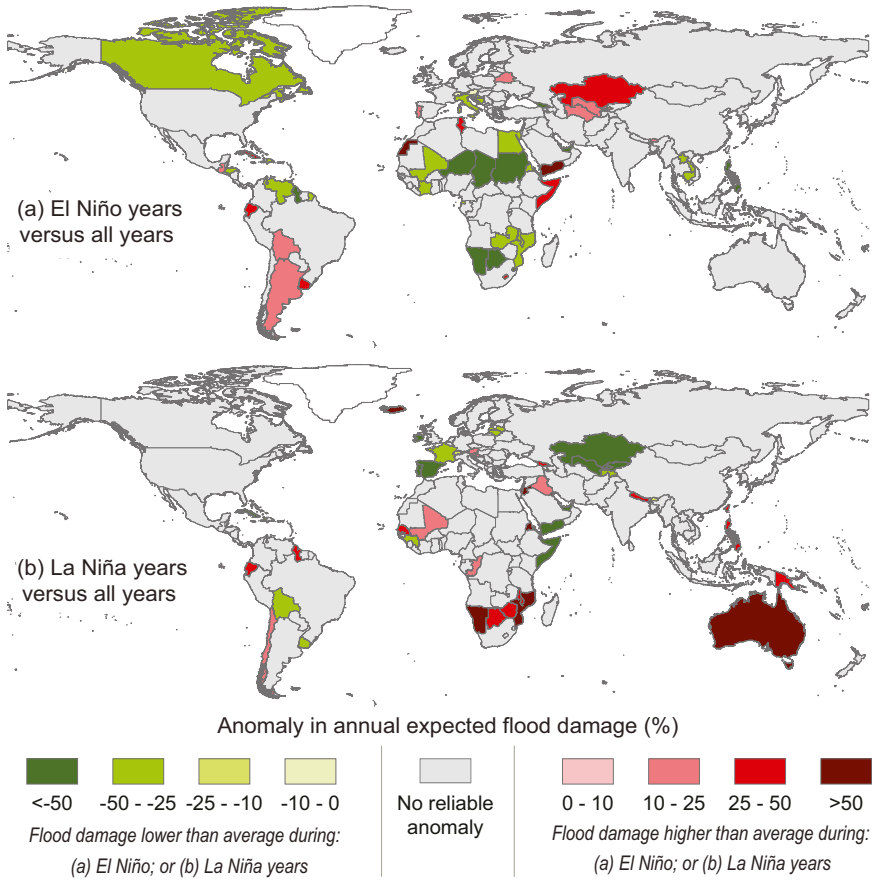

Fig. S6. Percentage anomaly per country in annual expected damage in urban areas for (*A*) El Niño years and (*B*) La Niña years (compared with all years). The results show the importance of the aggregation scale on the overall results in terms of anomalies in risk. Comparing the results at the country scale with those at the FPU scale shown in Fig. 2 shows that country-scale assessments mask important regional ENSO influences on risk. This is especially the case in larger countries where there are regionally opposite influences of ENSO on hydroclimate. A clear example is the United States: Based on the country-aggregated results, there is no reliable anomaly in this country during El Niño or La Niña years, yet the regionally disaggregated influence is high.

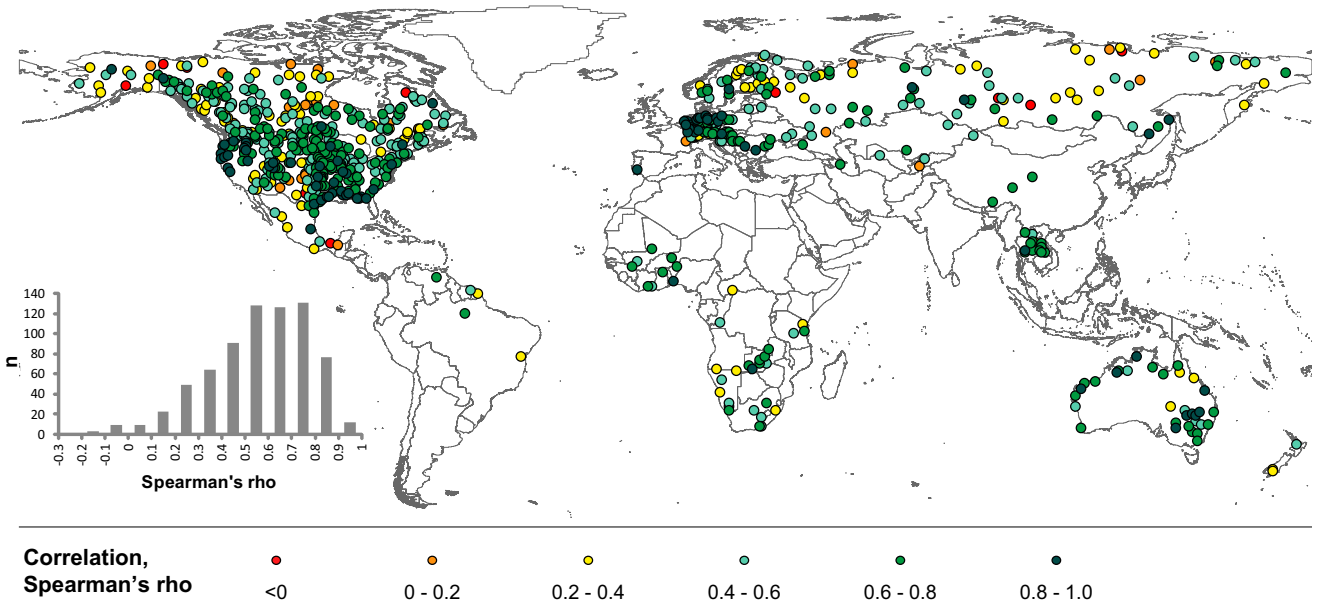

Fig. S7. Correlation (Spearman's rank, rho) between modeled and observed Q_{max} time series over the period 1958–2000. (*Inset*) Histogram of values for individual gauging stations, $n = 722$. For a discussion of these validation results, see *SI Discussion*, *Validation of Hydrological and Hydraulic Models*).

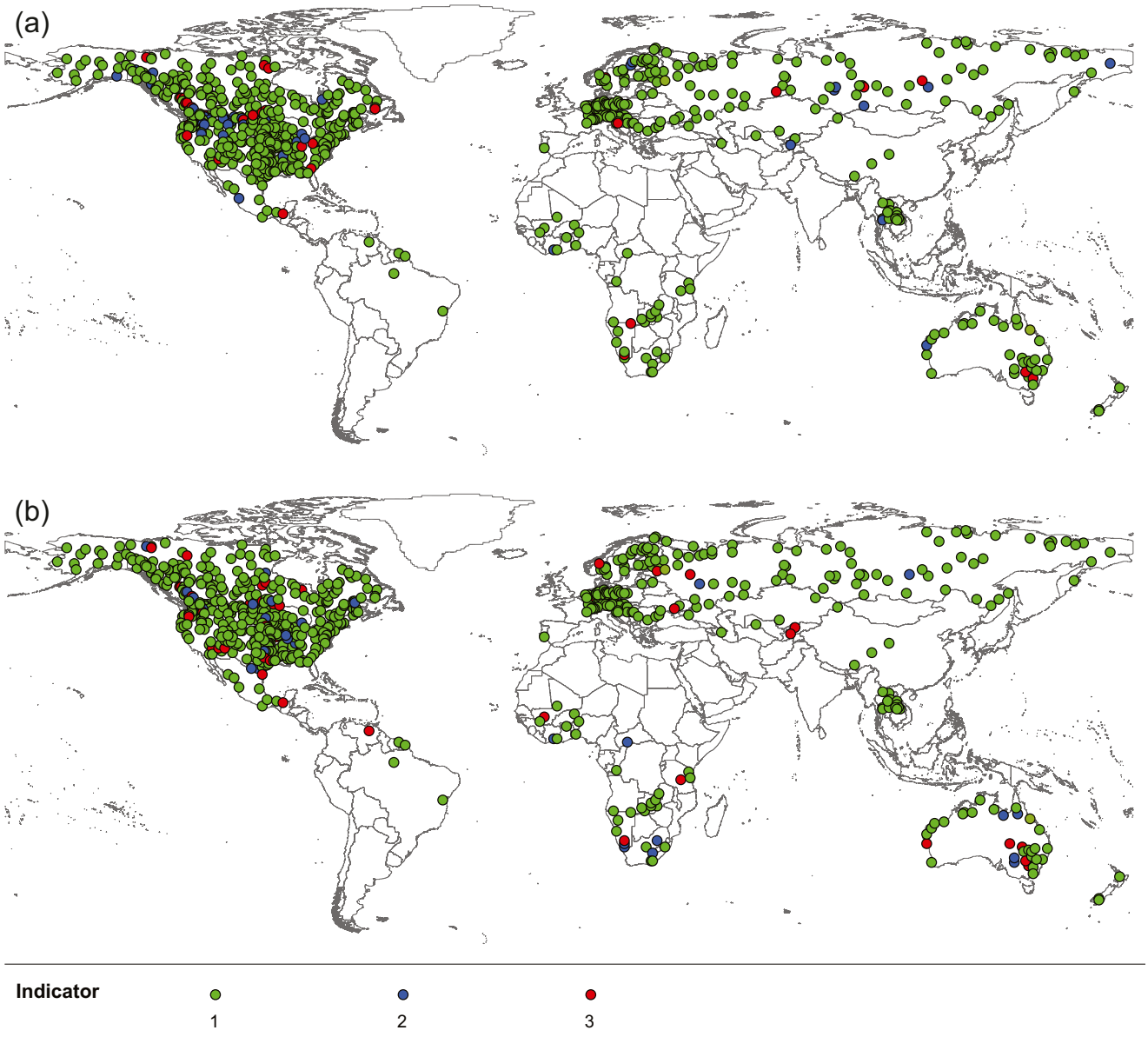

Fig. S8. Indicator of the agreement between modeled and observed median Q_{max} for (*A*) El Niño years compared with non-El Niño years and (*B*) La Niña years compared with non-La Niña years. Indicator 1 means that both modeled and observed median Q_{max} show either no significant difference or significant differences with the same sign. Indicator 2 means that modeled median Q_{max} shows no significant difference, whereas the observed Q_{max} does show a significant difference. Indicator 3 means that observed median Q_{max} shows no significant difference, whereas modeled Q_{max} does show a significant difference. There are no stations at which modeled and observed median Q_{max} show significant differences with the opposite sign. Statistical significance was assessed using a two-tailed Mann–Whitney *U* test, $\alpha = 0.05$. For a discussion of these validation results, see *SI Discussion*, *Validation of Hydrological and Hydraulic Models*.

Table S1. Percentage of land area (excluding Antarctica and Greenland) with reliable positive and negative anomalies in flood risk during El Niño and La Niña years

	El Niño		La Niña	
Flood risk indicator	Positive anomaly	Negative anomaly	Positive anomaly	Negative anomaly
Urban damage	10	19	10	13
Exposed GDP	12	39	13	30
Exposed population	12	38	14	30

Table S2. Percentage anomalies in globally aggregated values of modeled annual expected urban damage based on El Niño and La Niña years only (compared with results based on all years)

	Anomaly per ENSO phase, %	
Protection standard, y	El Niño	La Niña
2	−8.9	−14.2
5	−6.8	−10.9
10	−6.2	−9.8
25	−6.0	−8.9
50	−5.8	−8.7
100	−5.9	−8.8
250	−5.8	−8.9
500	−5.9	−9.0

Results are shown for different assumptions of a nominal protection standard (expressed as a return period) against flooding. None of the anomalies is reliable. The simulations carried out for this paper assume that no infrastructural flood protection measures are in place, such as dikes and retention areas. A past study has shown that the absolute risk estimates are strongly influenced by the assumed flood protection standard (1). Here, we assessed how anomalies in risk between ENSO phases are affected by assuming different nominal flood protection standards. At the global scale, we found that the flood protection standard has a fairly small influence on the simulated risk anomalies.

Table S3. Correlation (Spearman's rank, rho) between reported impacts (13) and modeled impacts over the period 1990–2000

Country	*n*	Spearman's rank, rho	
		Reported losses vs. urban damage	Reported fatalities vs. exposed population
Australia and Oceania	69	0.71	0.48
Central America	69	0.42	0.21
Eastern Asia	102	−0.03	0.52
Eastern Europe and Central Asia	123	0.24	−0.08
Indian subcontinent	131	0.15	0.32
Latin America	108	0.60	0.61
Middle East	71	0.50	0.81
Middle and South Africa	123	0.65	0.49
North Africa	32	−0.10	−0.18
North America	126	0.77	0.59
Southeastern Asia	127	0.62	0.77
Western Europe	140	0.70	0.68

Values are shown for the geographical regions shown in ref. 12. *n* is the number of reported events in the period used in the analysis. For a discussion of these results, see *SI Discussion*, *Validation of Hydrological and Hydraulic Models*.

Table S4. Correlation (Spearman's rank, rho) between reported impacts (13) and modeled impacts over the period 1990–2000 per country

Country	*n*	Spearman's rank, rho	
		Reported losses vs. urban damage	Reported fatalities vs. exposed population
United States	87	0.71	0.53
China	54	0.70	0.58
India	47	0.19	0.22
Russian Federation	45	0.15	−0.07
Canada	39	0.72	0.37
Indonesia	38	0.27	0.78
Australia	34	0.68	0.37
Brazil	32	0.42	0.50
Bangladesh	28	0.54	0.52
South Africa	27	0.63	0.51

Values are shown for the 10 countries with the largest number of observed flood events (*n*). For a discussion of these results, see *SI Discussion*, *Validation of Hydrological and Hydraulic Models*.